Coexistence of free excitonic matter with exciton magnetic polarons in $Cd_{1-x}Mn_xTe$ under nonresonant two-photon excitation

J. I. Jang,* S. Mani, and J. B. Ketterson†
Department of Physics and Astronomy, Northwestern University, 2145 Sheridan Road, Evanston, Illinois 60208, USA

H. Y. Park‡
Department of Semiconductor Applications, Ulsan College, San 29 Mugeo Dong, Ulsan 680-749, Republic of Korea
(Received 12 April 2008; published 17 June 2008)

Coexistence of free excitonic matter with exciton magnetic polarons (EMPs) in dilute magnetic semiconductors (DMSs) of $Cd_{1-x}Mn_xTe$ for $0.04 \leq x \leq 0.36$ is demonstrated at superfluid He temperatures under nonresonant two-photon excitation. Unlike conventional one-photon excitation, both free excitons and biexcitons are observed employing this excitation method at $x=0.04$. Bose stimulation of biexcitons and a metal-insulator Mott transition are also observed under strong excitation. For $x \geq 0.2$, only free excitons coexisting with EMPs are observed, which also exhibit stimulated emission under strong excitation. This implies that the Mn composition is an important kinematic parameter that affects the stability of biexcitons. Our results imply that a typical DMS system can exhibit strong optical phenomena, presumably correlated with various interesting magnetic effects, depending on excitation conditions.

DOI: 10.1103/PhysRevB.77.235211 PACS number(s): 75.50.Pp, 71.30.+h, 71.35.−y, 78.45.+h

I. INTRODUCTION

$Cd_{1-x}Mn_xTe$ is an extensively studied dilute magnetic semiconductor (DMS) both theoretically and experimentally.[1,2] The crystal structure is zinc blende (cubic with no inversion symmetry). Both the electron and hole band extrema are located at the zone center with a dipole-allowed gap $E_{gap}(x)$ that increases with the Mn composition x up to the band-gap pinning regime.[3,4] In this semimagnetic semiconductor, the exchange interaction between optically generated carriers and Mn^{2+} cations results in a large Zeeman splitting of energy levels,[5] giant Faraday rotation,[6] and exciton magnetic polaron (EMP) effects.[2] In low dimensional quantum structures based on this DMS, numerous interesting features have also been observed including coherent spin dynamics,[7] room-temperature polariton lasing,[8] and Bose-Einstein condensation of two-dimensional (2D) microcavity polaritons.[9] Recently, the renewed interest for DMSs was motivated by further applications involving information storage and processing based on spintronic devices.[10]

One of the most interesting magneto-optical properties mentioned above is photoinduced ferromagnetic spin alignment in paramagnetic $Cd_{1-x}Mn_xTe$ due to the localization of free excitons (electron-hole bound states) by ambient Mn^{2+} cations and impurities, namely, the formation of EMPs. The mechanisms for this localized magnetic transition within an exciton Bohr radius have been experimentally investigated using various spectroscopic methods under one-photon band-to-band excitation.[2] This excitation method initially generates free carriers subsequently forming EMPs. The two main EMP photoluminescence (PL) lines observed from $Cd_{1-x}Mn_xTe$ for $0<x<0.4$ were attributed to the so-called L_1 and L_2 lines, each arising from excitons bound to neutral acceptors and magnetically "self-trapped" excitons, respectively.[11] Based on the observed asymmetry of the L_2 line as a function of temperature, Takeyama *et al.*[12] further confirmed that the L_2 line consists of two components: (i) pointlike exciton localization under alloy potential fluctuations (APFs) and (ii) hole localization with the other constituent (an electron) simply bound by a screened Coulomb attraction. The latter corresponds to the intrinsic spin-induced localization of excitons since it primarily arises from a pure spin-spin interaction between the host $5p$-hole and $3d-Mn^{2+}$ electronic states. This EMP effect was also well studied in other DMS materials, but there has been no spectroscopic evidence of free excitonic matter in this system.

In this paper, we report the first observation of free excitonic matter in conventional DMS, $Cd_{1-x}Mn_xTe$, at 2 K under *nonresonant two-photon excitation* that selectively generates free excitons via an impurity band transition. The associated intermediate state is most likely formed by random magnetic impurities and APFs in this DMS. Nonresonant two-photon transition is a rather well established phenomenon in *direct-gap* semiconductors containing sufficient impurity concentrations, where direct generation of excitons is allowed via two-photon pumping to an intermediate impurity band subsequently decaying into the ground state of free excitons.[13–15] In our $Cd_{1-x}Mn_xTe$, we found that this two-photon transition persists over a broad range of excitation energies almost spanning from the two-photon to one-photon exciton resonance energy for a given x. The observed PL spectra for different excitation energies in this range indicate that the corresponding two-photon absorption coefficient, $\beta(\varepsilon_{2p})$, monotonically increases with the two-photon excitation energy ε_{2p}.

This paper is organized as follows: The experimental setup for the measurement is described in Sec. II. In Sec. III the observed PL spectra under two-photon excitation are compared with those obtained under one-photon excitation at $x=0.04$. The additional peaks under two-photon excitation are identified based on the steady-state population dynamics. Various free excitonic phases under strong excitation levels are discussed in Sec. IV. In Sec. V we discuss free exciton generation and stimulated emission for $x \geq 0.2$ under the

same excitation conditions. Summary and conclusions are given in Sec. VI.

II. EXPERIMENTAL SETUP

Our PL measurements were performed on four bulk $Cd_{1-x}Mn_xTe$ samples ($x=0.04$, 0.2, 0.285, and 0.36), which were grown using the vertical Bridgman method. Samples were cut and polished along the growth direction and the corresponding thickness of each sample was about 1 mm. These samples were mounted in an optical cryostat and cooled to 2 K in a Janis variable-gas-flow optical cryostat. We use the frequency-tripled output of a passive-active mode-locked EKSPLA PL 2143 series Nd doped yttrium aluminum garnet (YAG) laser with a pulse width of about 15 ps and a repetition rate of 10 Hz to synchronously pump an optical parametric amplifier (OPA). The OPA generates vertically polarized pulses in the range of 400–3100 meV.

The incident laser pulse from the OPA was focused onto each sample surface using a 15 cm focal-length lens. The corresponding photon flux P was varied from 0.2 to 68.2 mJ/cm^2. The excitation energies were tuned to $\varepsilon_{1p}=2420$ meV and $\varepsilon_{2p}=1072$ meV for one-photon and two-photon excitations, respectively. The PL was collected in a transmission geometry from the opposing surface and focused onto a fiber-optic bundle. The output of the fiber-optic bundle was coupled to the entrance slit of a Spex Spec-One 500 M spectrometer and detected using a nitrogen-cooled charge-coupled device (CCD) camera. Although there were noticeable variations in the PL intensities, we confirmed that the corresponding spectral features under both excitation methods barely depend on not only the excitation position but also the excitation energy that determines the absorption length.

III. PHOTOLUMINESCENCE AT $x=0.04$

The solid trace in Fig. 1(a) illustrates the typical time-integrated PL spectrum at 2 K obtained from our $Cd_{0.96}Mn_{0.04}Te$ sample under one-photon over-the-gap excitation ($\varepsilon_{1p}=2420$ meV), clearly showing the L_1 and L_2 lines typical of EMPs either bound to neutral acceptors or self-trapped in the vicinity of Mn^{2+} cations. The spectral positions of these peaks are approximately consistent with the previous results described elsewhere.[16] These EMP PL lines are usually very broad even at 2 K because of the inhomogeneous line broadening arising from APFs and spatial inhomogeneity of the sample. We found that the spectral features of the L_1 and L_2 lines barely depend on the one-photon excitation power [see Fig. 6(a)].

On the other hand, the dashed trace in Fig. 1(a) corresponds to the time-integrated PL spectrum when the sample is now excited by $\varepsilon_{2p}=1072$ meV laser light. It is interesting to notice that the additional two sharp peaks E and M appear for an excitation energy far below the band gap, implying that a multiphoton process is involved. The heavy red trace is obtained by subtracting the solid trace from the dashed trace in order to investigate the population of the E and M lines only. As verified and shown later, these two PL lines arise

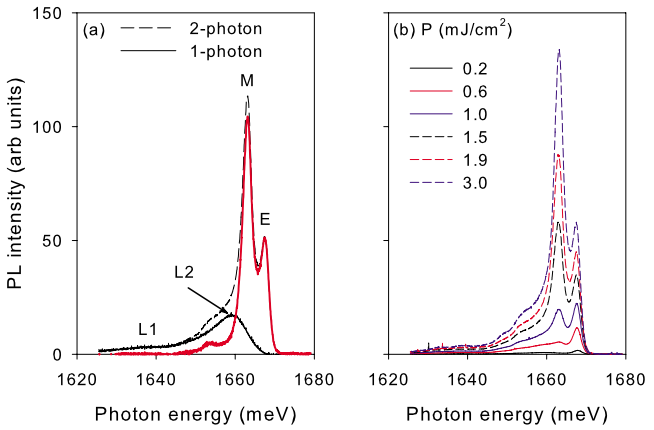

FIG. 1. (Color online) (a) Time-integrated PL spectra at 2 K obtained from $Cd_{1-x}Mn_xTe$ at $x=0.04$ under one-photon (solid trace) and two-photon (dashed trace) excitations, respectively. The solid trace is properly scaled to match with the lower-energy tail of the dashed trace. For ordinary one-photon excitation, the PL shows two broad peaks L_1 and L_2. The additional two peaks observed under two-photon excitation correspond to the free exciton (E) and biexciton (M) PL lines, respectively. The heavy red trace shows the PL spectrum after subtracting the contribution from EMPs. (b) Time-integrated PL spectra for various excitation intensities in the range of 0.2–3.0 mJ/cm^2.

from radiative recombination of *free* excitons and biexcitons (excitonic molecules), respectively, generated by two-photon excitation.

Figure 1(b) shows plots of several time-integrated spectra for various excitation intensities ($P=0.2$–3.0 mJ/cm^2) under two-photon excitation, clearly indicating that free excitonic matter coexists with EMPs. Note that the relative population for E and M strongly depends on the two-photon excitation power. Considering that ordinary one-photon excitation to charged carriers does not show these PL lines from free excitonic matter, the EMP formation (magnetic interaction) time for the carriers should be at least comparable with the time scale for the free exciton formation (Coulomb interaction).

Figure 2(a) corresponds to the time-integrated PL spectra shown in Fig. 1(b) after subtracting the contribution from the EMP PL lines. The measured spectral position of the free exciton line is about 1667.2 meV. This value is slightly larger than the predicted value from the empirical formula at $x=0.04$, which is indirectly determined by the absorption measurements.[16] At the minimum excitation level, $P=0.2$ mJ/cm^2, the E line is mostly dominant, implying that free excitons are initially created. As the excitation power increases, the M line appears and develops faster than the E line. Unlike the symmetric E line, the M line is well fit by an *inverted* Boltzmann distribution at $T\simeq 2$ K, unambiguously indicating that it arises from radiative recombination of free biexcitons.[17] The corresponding biexciton binding energy is about 4.3 meV. This value is somewhat larger than the measured binding energy in CdTe, which is determined by the energy difference between bound excitons and bound biexcitons (or bound multiexcitonic complex) captured by ubiquitous impurities.[18] The PL line denoted by BE near 1653 meV

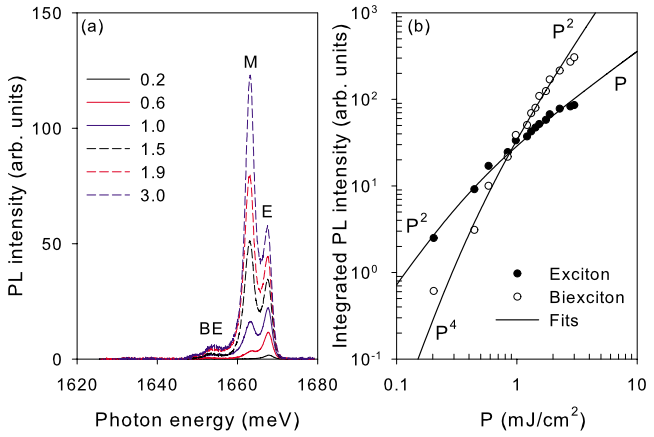

FIG. 2. (Color online) (a) Time-integrated PL spectra from Fig. 1(b) after the background subtraction, showing the free exciton (E), biexciton (M), and bound exciton (BE) PL, respectively. (b) Spectrally integrated PL intensities for excitons (dots) and biexcitons (circles) from part (a). The superimposed solid curves are the steady-state solutions to the rate equations, clearly indicating that free excitons are initially generated under nonresonant two-photon excitation. The approximate excitation-power dependences are also shown for both low- and high-excitation limits.

is attributed to the bound exciton PL based on the same power dependence as that for free excitons.[19]

We now explicitly show that the observed PL intensities from each free excitonic matter follow the predicted population dynamics under two-photon excitation. Similar to the ordinary resonant case, where the two-photon absorption coefficient is an intrinsic constant quantity, the nonresonant two-photon absorption coefficient can be parametrized by $\beta(\varepsilon_{2p})$ for a given ε_{2p} and defined by

$$\frac{dP(z)}{dz} = -\beta(\varepsilon_{2p})P^2(z), \tag{1}$$

where $P(z)$ is the two-photon attenuation of the incident photon flux inside the crystal. The corresponding depth distribution $G(z)$ for the excitonic matter created matches the laser absorption profile and is given by[20]

$$G(z) = -\frac{1}{2}\frac{dP(z)}{dz} = \frac{1}{2}\frac{\beta(\varepsilon_{2p})P(0)^2}{[P(0)\beta(\varepsilon_{2p})z+1]^2}, \tag{2}$$

where $P(0)=P$ is the photon flux at the surface. As described in Sec. II, however, our collection geometry ensures that the observed PL is spatially integrated. Therefore, the measured generation rate G is not a function of the z but should be obtained by averaging Eq. (2) with respect to z, which is simply given by $\beta(\varepsilon_{2p})P^2$.

The simultaneous rate equations describing the free exciton density (n) and biexciton density (n_b) are given by

$$\frac{dn}{dt} = -\frac{n}{\tau} + \frac{n_b}{\tau_b} - 2Cn^2 + 2Cn^*(T)n_b + G, \tag{3}$$

and

$$\frac{dn_b}{dt} = -\frac{n_b}{\tau_b} + Cn^2 - Cn^*(T)n_b, \tag{4}$$

where τ is the overall exciton lifetime including the radiative decay and EMP formation times, τ_b is the biexciton radiative lifetime, and C is the exciton–exciton capture coefficient to form a biexciton; $n^*(T)$ is the mass-action equilibrium constant that depends on temperature and is given by

$$n^*(T) = \left(\frac{M_b k_B T}{8\pi\hbar^2}\right)^{3/2} e^{-E_b/k_B T}, \tag{5}$$

where M_b and E_b are the biexciton mass and binding energy. The terms Cn^2 and $-Cn^*(T)n_b$ in Eq. (4) correspond to biexciton formation and dissociation, respectively. Considering a relatively strong biexciton binding energy of 4.3 meV, however, thermal dissociation of a biexciton at 2 K is quite negligible, $n^*(2\mathrm{K}) \ll n^2/n_b$.[21]

The steady-state solutions for the free exciton and biexciton densities are related to the measured PL intensities I and I_b by

$$I = \frac{n}{\tau} = 2G_o\left(\sqrt{1+\frac{G}{G_o}} - 1\right), \tag{6}$$

and

$$I_b = \frac{n_b}{\tau_b} = G_o\left(\sqrt{1+\frac{G}{G_o}} - 1\right)^2, \tag{7}$$

where the characteristic generation rate G_o is defined by $G_o=(4C\tau^2)^{-1}$. Although n_b is always proportional to n^2, the exciton density n, thus I, is *not* directly proportional to the exciton generation rate G in the steady-state regime. As predicted from Eq. (6), the measured exciton PL intensity I increases sublinearly as $G^{1/2}$ for $G \gg G_o$ [see the solid curves in Fig. 2(b) for the two-photon excitation case].

In Fig. 2(b) we plot the spectrally integrated PL intensities for excitons (dots) and biexcitons (circles) from Fig. 2(a). The superimposed solid curves correspond to Eqs. (6) and (7) and are generated by assuming $G=\beta(\varepsilon_{2p})P^2$ and properly choosing G_o and $\beta(\varepsilon_{2p})$ at $\varepsilon_{2p}=1072$ meV.[22] The observed steady-state population dynamics unambiguously show that free excitons are initially created under this rather unconventional two-photon excitation. Although ε_{2p} is not exactly resonant with the free exciton internal energy, this higher-order transition into the ground-state free excitons has been shown to occur in random or single-crystal semiconductors with a high impurity concentration.[13–15] We emphasize that this two-photon transition is very different from usual over-the-gap two-photon excitation that again initially generates charged carriers. Otherwise, the observed PL should be just the same as that obtained under one-photon over-the-gap excitation, which does not show any PL from free excitonic matter.

IV. BOSE STIMULATION OF BIEXCITONS AND MOTT TRANSITION

We also find that additional interesting phenomena related to high-density free excitonic matter are observed from our

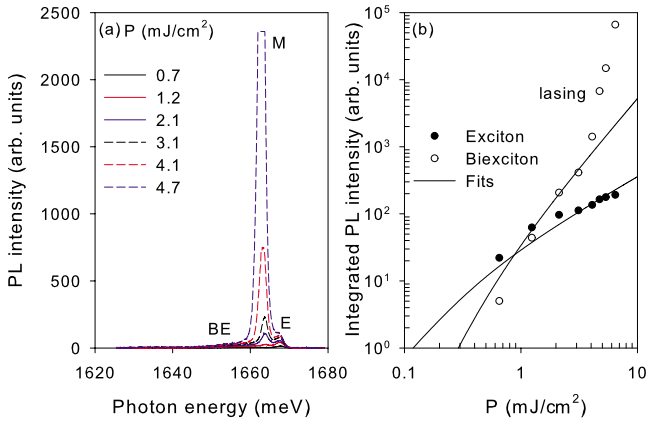

FIG. 3. (Color online) (a) Time-integrated PL spectra for higher excitation levels (P=0.7–4.7 mJ/cm^2) under the same excitation conditions. (b) Spectrally integrated exciton and biexciton PL intensities are plotted by dots and circles, respectively. The solid curves are the same curves in Fig. 2(b). Rapid increase in the M line strongly indicates Bose stimulation of biexcitons for P >3.1 mJ/cm^2.

$Cd_{0.96}Mn_{0.04}Te$ sample under nonresonant two-photon excitation. Figure 3(a) shows several time-integrated spectra for excitation powers in the range of 0.7–4.7 mJ/cm^2 under the same excitation conditions. The rapid growth of the M line clearly indicates stimulated biexciton emission with a threshold of about P_c=3.1 mJ/cm^2. The corresponding spectrally integrated PL intensities for excitons (dots) and biexcitons (circle) are plotted in Fig. 3(b), superimposed by the fits (solid curves) using the parameters determined at lower excitation levels. Note that we observe a significant deviation of the biexciton population above the threshold, whereas the exciton population approximately follows the theoretical prediction. Obviously, above this threshold, the biexciton population cannot be simply described by classical simultaneous rate equations that do not take into account the corresponding Bose occupation number. Considering that most stimulated emission phenomena observed in DMS-based quantum structures arise from polariton lasing,[8] it is rather interesting to observe similar behavior associated with biexcitons in our bulk $Cd_{1-x}Mn_xTe$ sample at x=0.04.

Figure 4(a) shows the evolution of the PL spectra when the excitation intensity is further increased from 5 to 50 mJ/cm^2 under the same excitation conditions. The apparently much broader biexciton peaks basically arise from time integrating the actually sharper M lines that continuously undergo a *band-gap shift* with time due to the so-called mean-field band-gap renormalization. Also, note that Bose amplification of the biexciton PL is significantly suppressed for P>20 mJ/cm^2. This primarily arises from a many-body interaction between excitonic matter constituents due to enhanced Coulomb screening, favoring a new quantum phase above a threshold associated with the Mott density. Above the Mott density, electrons and holes no longer possess pairwise correlation, and therefore, charge neutral excitons and biexcitons ionize into the metallic electron-hole plasma (EHP). This EHP phase becomes increasingly fermionic with increasing intensity and hence we expect quenching of Bose amplification.

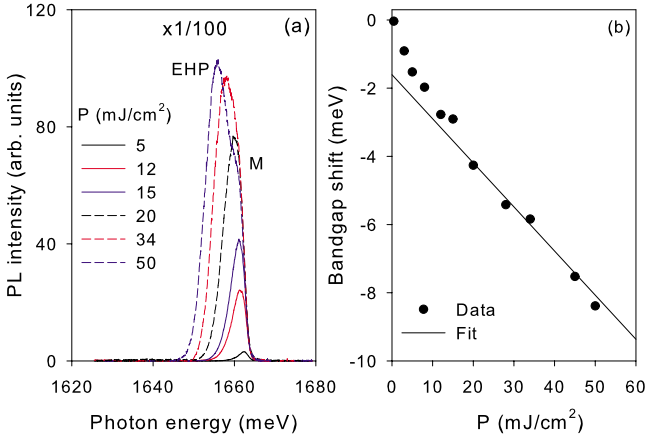

FIG. 4. (Color online) (a) Time-integrated PL spectra (100 times scaled down) at 2 K under very strong excitation levels in the range of 5–50 mJ/cm^2. The rapid biexciton population is much suppressed for P>20 mJ/cm^2. The evolution of the PL spectral features are detailed in the text. (b) Band-gap redshift (dots) determined by the maximum peak position as a function of the excitation power, superimposed by an empirical fit (solid line).

Figure 4(b) plots the measured band-gap shift (dots) arising from band-gap renormalization inferred from the maximum peak position at a given excitation intensity. The solid line is an empirical fit to the data above the Mott density based on the theoretical mean-field shift that is proportional to the density of excitonic matter. As expected, the density of EHP is proportional to the excitation power P in the steady-state regime under two-photon excitation and is, therefore, well explained by the empirical linear fit. The noticeable deviation below the Mott density arises from faster band-gap shift due to Bose stimulation as well as stronger excitation-power dependence at the lower excitation limit.

V. RESULTS FROM SAMPLES FOR $x \geq 0.2$

In this section, we extend our studies to other bulk $Cd_{1-x}Mn_xTe$ samples with higher Mn compositions. In Fig. 5 we plot the normalized time-integrated PL spectra at 2 K under one-photon excitation (ε_{1p}=2420 meV) at x=0.04 (pink), 0.2 (cyan), 0.285 (green), and 0.36 (yellow), respectively. For $x \leq 0.2$ the spectral positions for these two lines are rather close and can be more clearly resolved using polarization-dependent time-resolved spectroscopy.[23] The solid line corresponds to the empirical formula describing the band-gap shift as a function of Mn composition x; E_{L_2} =1604.7+1397x meV.[16]

Figure 6(a) plots several time-integrated PL spectra at 2 K from $Cd_{1-x}Mn_xTe$ for x=0.285 under one-photon excitation for excitation powers in the range of 11.1–43.6 mJ/cm^2. At this Mn composition or higher, the L_1 line is very broad as indicated by its high-energy tail, extending into the L_2 line. Note that the spectral features of these EMP lines barely depend on the one-photon excitation power. Figure 6(b) shows time-integrated PL spectra under the same conditions but the sample is now excited using two-photon excitation. With the solid line as a guide, representing the spectral po-

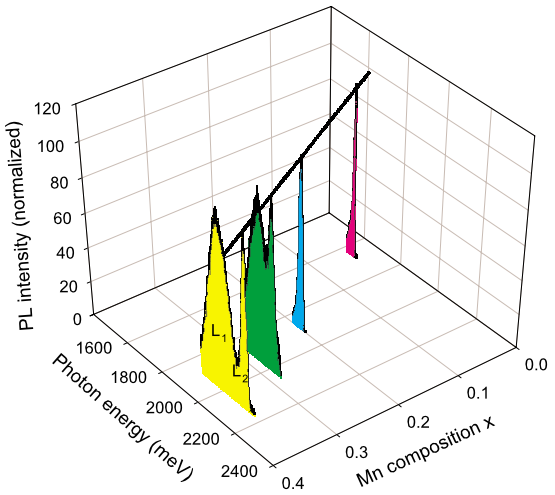

FIG. 5. (Color online) Typical time-integrated EMP PL at 2 K from $Cd_{1-x}Mn_xTe$ for $0.04 \leq x \leq 0.36$ under one-photon excitation. Each PL intensity is normalized for comparison. The solid line corresponds to the predicted spectral position of the L_2 line as a function of x.

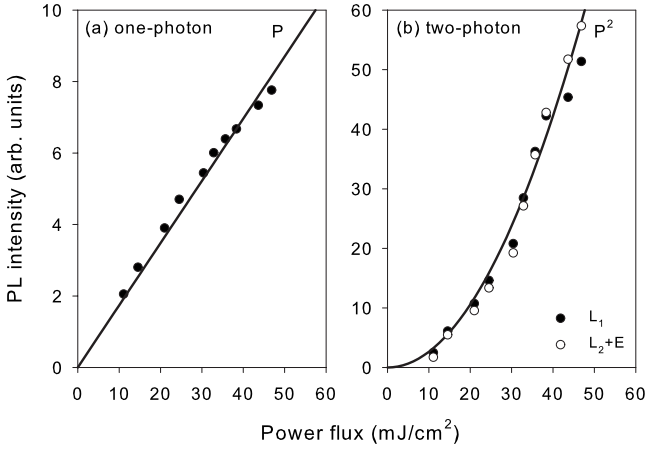

FIG. 7. The corresponding L_1 peak intensities (dots) under (a) one-photon excitation and (b) two-photon excitation are superimposed by linear and quadratic fits. The circles correspond to the L_2+E peak intensities properly scaled, showing the same power dependence.

sition of the L_2 line under one-photon excitation, it is interesting that the L_2 line apparently shifts toward higher energies with a significantly increased PL intensity, compared with the one-photon excitation case. As clearly shown in Fig. 8(a) and explained later, this basically arises from a strong free exciton peak (E) on top of this EMP PL line. These two peaks are not spectrally resolvable due to a substantial inhomogeneous broadening, intrinsic to alloy compounds for a high substitution rate x. Considering that a two-photon transition is a higher-order process, it is rather surprising that this two-photon excitation yields much more efficient EMP generation.

The dots in Fig. 7(a) correspond to the L_1 peak intensities at a given excitation power obtained from Fig. 6(a). The solid line is a linear fit to the data. From Fig. 6(a), it is obvious that the L_2 line also increases linearly with the excitation power, indicating that EMPs are generated under one-photon excitation. The corresponding L_1 peak intensities (dots) under two-photon excitation obtained from Fig. 6(b) are plotted in Fig. 7(b). The excitation-power dependence of the L_1 line is well described by a *simple* P^2 fit (solid curve) for two-photon excitation. The circles in Fig. 7(b) correspond to the combined peak L_2+E intensities, indicating that the E intensity also has the same power dependence. This is in sharp contrast to the case observed from our $Cd_{0.96}Mn_{0.04}Te$ sample, exhibiting a rather complicated power dependence given by Eq. (6) and corresponding to the special case $C=0$. As will be discussed later, this implies that free biexcitons are not stable as evidenced by the absence of the M line in the PL spectra shown in Fig. 6(b). We found that two other samples with different x show similar spectral features with the same power dependence for both excitation methods.

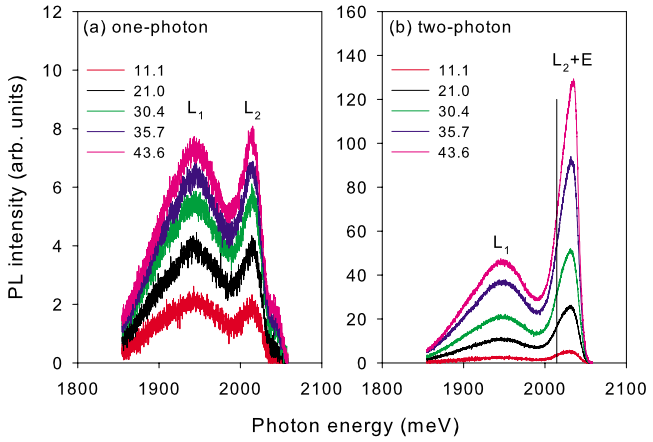

FIG. 6. (Color online) (a) Time-integrated PL spectra at 2 K from $Cd_{0.715}Mn_{0.285}Te$ under one-photon excitation for several excitation powers. (b) Time-integrated PL spectra under the same conditions using nonresonant two-photon excitation. The solid line is the spectral position for the L_2 line determined under one-photon excitation. Note that the L_2 line overlaps with the free exciton line (E), as indicated by an apparent blueshift of the combined peak.

Figure 8(a) shows a series of the two-photon spectra for higher excitation powers in the range of 19.7–68.2 mJ/cm^2 under the same excitation conditions. Note that the rapid growth of the E line occurs when the excitation power is larger than $P_c=43.6$ mJ/cm^2. The measured spectral position of the free exciton PL line is about 2038.7 meV, which is approximately consistent with the prediction, $E_E=1588+1584x$, obtained from the electroreflectance data.[24] The corresponding free exciton PL intensities (dots), after subtracting the EMP contributions, are plotted in Fig. 3(b) for $11.1 \leq P \leq 68.2$ mJ/cm^2. The solid line corresponds to a quadratic fit on the log-log scale, indicating that the free exciton population exponentially increases above the threshold power P_c.

Figure 9(a) shows the typical E lines on top of the L_2 EMP PL at 2 K obtained under strong excitation, showing stimulated emission of free excitons in $Cd_{1-x}Mn_xTe$ at $x=0.2$ (red traces), 0.285 (green traces), and 0.36 (blue traces), respectively. The dashed traces correspond to the PL spectra

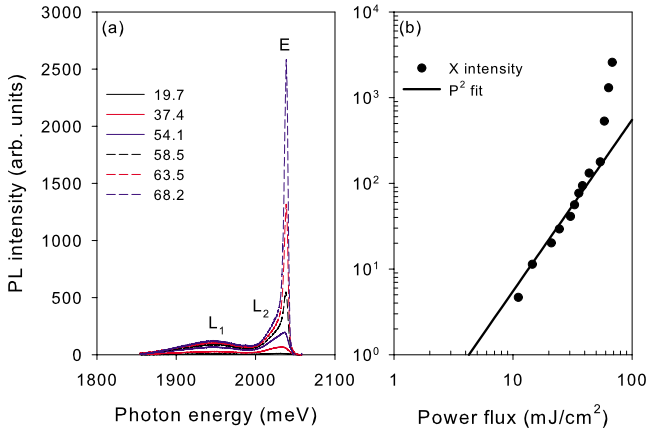

FIG. 8. (Color online) (a) Time-integrated PL spectra for higher excitation levels (P=19.7–68.2 mJ/cm^2) under the same excitation conditions. (b) The free exciton PL intensities are plotted as the dots and superimposed by a fit proportional to P^2. A rapid increase in the E line arises from stimulated emission of free excitons for $P>43.6$ mJ/cm^2.

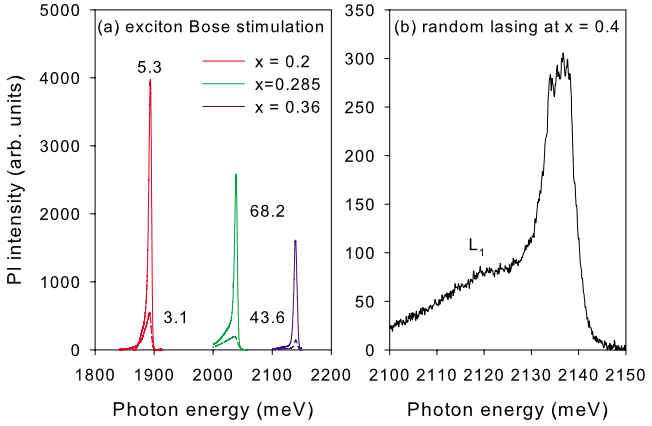

FIG. 9. (Color online) (a) Stimulated emission of free excitons in $Cd_{1-x}Mn_xTe$ at 2 K under nonresonant two-photon excitation at x=0.2 (red traces), 0.285 (green traces), and 0.36 (blue traces), respectively. The dashed traces correspond to each L_2+E line at the thresholds of P_c=3.1 (x=0,2) and 43.6($x\geq$0.285) mJ/cm^2. The solid traces correspond to the PL spectra at P=5.3 and 68.2 mJ/cm^2, respectively. (b) Random lasing behavior at P =58.5 mJ/cm^2 from a low-quality $Cd_{0.6}Mn_{0.4}Te$ sample under nonresonant two-photon excitation.

at the thresholds of P_c=3.1 and 43.6 mJ/cm^2, respectively. It is interesting that the two-photon absorption efficiency drastically decreases by a factor of 15 for $x\geq$0.285 compared with that at x=0.2. This can be partially explained by the two-photon absorption coefficient that increases with $\delta E=E_{gap}(x)-\varepsilon_{2p}$ but most likely arises from the loss of the optical efficiency induced by higher Mn substitution rates, which inevitably increases more impurities and APFs. The solid traces show a dramatic increase in the E line intensities at P=5.3 and 68.2 mJ/cm^2, which is slightly larger than P_c.

Unlike a very dilute $Cd_{0.96}Mn_{0.04}Te$ sample hosting both free excitons and biexcitons as shown in Fig. 2, we found that the biexciton phase is unstable in this DMS for $x\geq$0.2, and therefore, Bose stimulation is associated with free excitons, not biexcitons. This is also supported by the observed free exciton population that increases with P^2. Otherwise, its power dependence would deviate from P^2 and evolve into P with the excitation power due to the efficient *two-body* molecule formation process [see Fig. 2(b)].[14,15,21] This presumably arises from (i) an enhanced exchange interaction that efficiently aligns the exciton spin, rendering the exciton–exciton interaction repulsive or (ii) a magnetic phase transition into spin glass[25] for $x\geq$0.2. At this time, the origin for the suppression of biexciton formation is not clear.

We also performed similar two-photon excitation experiments on $Cd_{1-x}Mn_xTe$ at x=0.4, which has a rather low sample quality. As shown in Fig. 9(b), the stimulated free exciton line splits into several discrete lasing modes at P =58.5 mJ/cm^2. This random lasing behavior[26] is quite special in that feedback is caused by light scattering due to randomly distributed scatterers, not by light reflection by cavity mirrors in conventional lasing. As opposed to four samples with a high sample quality, which were mainly used in our experiments, we found that the observed spectral features from this low-quality sample strongly depend on the excitation positions.

VI. SUMMARY AND CONCLUSIONS

In conclusion, we observed free excitonic matter coexisting with typical EMPs in $Cd_{1-x}Mn_xTe$ for $0.04\leq x\leq 0.36$ at 2 K under nonresonant two-photon excitation that initially generates free excitons. This effect was not observed under the usual one-photon excitation of charged carriers. Based on the steady-state population dynamics, the evolution of the PL lines from free excitonic matter was studied as a function of the excitation power. In $Cd_{0.96}Mn_{0.04}Te$, all possible free excitonic phases including biexcitons, Bose stimulation, and the EHP were observed under this excitation method. For x $\geq$0.2, however, only free excitons coexisting with EMPs were observed. Bose stimulation of free excitons was also observed under strong two-photon excitation. Based on our extensive studies, we believe that the Mn concentration x is an important kinematic parameter, particularly with respect to the stability of biexcitons, in the semimagnetic semiconductor $Cd_{1-x}Mn_xTe$. Our new results demonstrate that the optical responses of $Cd_{1-x}Mn_xTe$ can strongly depend on the excitation method. Although the present work mostly highlighted free excitonic matter, we believe that further studies on both free excitonic matter and EMPs under two-photon excitation with various experimental parameters will improve the understanding of basic optical and magnetic properties of DMSs.

ACKNOWLEDGMENTS

This work is supported by the National Science Foundation under a U.S./Ireland corporation Grant No. 0306731 and by the Northwestern Materials Research Center under NSF Grant No. DMR-9632472.

*joon-jang@northwestern.edu
†j-ketterson@northwestern.edu
‡hypark@mail.uc.ac.kr

[1] J. K. Furdyna, J. Appl. Phys. **64**, R29 (1988).
[2] S. Takeyama, in *Magneto-Optics*, edited by S. Sugano and N. Kojima (Springer-Verlag, Berlin, 2000), and references therein.
[3] S. H. Wei and A. Zunger, Phys. Rev. B **35**, 2340 (1987).
[4] Y. R. Lee and A. K. Ramdas, Solid State Commun. **51**, 861 (1984).
[5] J. K. Furdyna, J. Appl. Phys. **53**, 7637 (1982).
[6] J. A. Gaj, R. R. Galazka, and M. Nawrocki, Solid State Commun. **25**, 193 (1978).
[7] A. Brunetti, M. Vladimirova, D. Scalbert, R. André, D. Solnyshkov, G. Malpuech, I. A. Shelykh, and A. V. Kavokin, Phys. Rev. B **73**, 205337 (2006).
[8] P. Alleysson, J. Cibert, G. Feuillet, and L. S. Dang, J. Cryst. Growth **159**, 672 (1996).
[9] J. Kasprzak, M. Richard, S. Kundermann, A. Baas, P. Jeambrun, J. M. Keeling, F. M. Marchetti, M. H. Szymańska, R. André, J. L. Staehli, V. Savona, R. B. Littlewood, B. Deveaud, and L. S. Dang, Nature (London) **443**, 409 (2006).
[10] See, for example, M. Oestreich, J. Hübner, D. Hägele, P. J. Klar, W. W. Rühle, D. E. Ashenford, and B. Lunn, Appl. Phys. Lett. **74**, 1251 (1999).
[11] A. Golnik, J. Ginter, and J. A. Gaj, J. Phys. C **16**, 6073 (1983).
[12] S. Takeyama, S. Adachi, Y. Takagi, and V. F. Aguekian, Phys. Rev. B **51**, 4858 (1995).
[13] D. C. Dai, S. J. Xu, S. L. Shi, M. H. Xie, and C. M. Che, Opt. Lett. **30**, 3377 (2005).
[14] J. I. Jang, M. A. Anderson, J. B. Ketterson, and R. P. H. Chang, Appl. Phys. Lett. **92**, 051912 (2008).
[15] J. I. Jang, M. A. Anderson, J. B. Ketterson, and R. P. H. Chang, J. Lumin. (to be published).
[16] D. Heiman, P. Becla, R. Kershaw, D. Ridgley, K. Dwight, A. Wold, and R. R. Galazka, Phys. Rev. B **34**, 3961 (1986), and references therein.
[17] A. Mysyrowicz, in *Bose-Einstein Condensation*, edited by A. Griffin, D. W. Snoke, and S. Stringari (Cambridge University Press, Cambridge, England, 1995).
[18] J. A. Wolk, T. W. Steiner, V. A. Karasyuk, and M. L. W. Thewalt, Phys. Rev. Lett. **50**, 18030 (1994).
[19] J. I. Jang, Y. Sun, B. Watkins, and J. B. Ketterson, Phys. Rev. B **74**, 235204 (2006).
[20] K. E. O'Hara and J. P. Wolfe, Phys. Rev. B **62**, 12909 (2000).
[21] For detailed chemical equilibrium dynamics between two species, see, for example, J. I. Jang and J. P. Wolfe, Phys. Rev. B **74**, 045211 (2006).
[22] The absolute values for these parameters cannot be determined without calibration of the actual density of excitonic matter.
[23] T. Okada and T. Itoh, J. Phys.: Condens. Matter **19**, 186210 (2007).
[24] J. Stankiewicz, N. Bottka, and W. Giriat, J. Phys. Soc. Jpn. **49**, 827 (1980).
[25] R. R. Galazka, S. Nagata, and P. H. Keesom, Phys. Rev. B **22**, 3344 (1980).
[26] See, for example, Y. Sun, J. B. Ketterson, and G. K. L. Wong, Appl. Phys. Lett. **77**, 2322 (2000).